International Journal on Magnetic Particle Imaging
Vol 7, No 2, Article ID 2109001, 8 Pages

Infinite Science Publishing

Research Article

Further system characterization of the Single-Sided MPI Scanner with two- and three-dimensional measurements

Yvonne Blancke Soares [a,*] · Kerstin Lüdtke-Buzug [a] · Anselm von Gladiss [a,b] · Christina Debbeler [a] · Thorsten M. Buzug [a,c] · Ksenija Gräfe [a,*]

[a] Institute of Medical Engineering, University of Lübeck, Lübeck
[b] now with: Active Vision Group, Institute of Computational Visualistics, University of Koblenz-Landau, Germany
[c] Fraunhofer Research Institution for Individualized and Cell-Based Medical Engineering, Lübeck, Germany
[*] Corresponding author, email: {soares,graefe}@imt.uni-luebeck.de

Received 26 October 2020; Accepted 07 September 2021; Published online 13 September 2021

Abstract

With the single-sided MPI-Scanner unlimited object sizes can be measured and it is suitable for various medical applications. In previous measurements, the penetration depth for two-dimensional measurements has already been investigated, as well as the local resolution. The system has evolved from a one-dimensional to a three-dimensional system. Here, further measurements are carried out to characterize the system. To measure the penetration depth and spatial resolution as well as the influence of the orientation of the receiving coils, a four-layer phantom was measured three-dimensionally at different angles. Furthermore, a dilution series was measured to determine the linearity of the system reaction, which is a prerequisite for the quantifiability of the results. The results of both studies are shown and discussed in this work.

I. Introduction

Magnetic particle imaging (MPI) uses the nonlinear magnetic behavior of superparamagnetic iron oxide nanoparticles (SPIOs) [1]. They are saturated by a homogeneous magnetic field and excited by the movement of a field-free region (FFR) across the field of view (FOV), which leads to a change in magnetization and induces a signal in the receiving coils. Certain frequencies are used to move the FFR on a trajectory that covers the entire FOV [2]. Only particles in or near the FFR are excited, which allows spatial encoding.

However, due to their design, the size of the object to be measured is limited, which led to the development of a single-sided MPI setup in 2009 [3]. Due to the single-sided arrangement of the coils it is possible to measure patients or objects of any size. However, due to field inhomogeneities, the penetration depth that can be achieved with a single-sided arrangement is limited. The detection of sentinel lymph nodes in patients suffering from breast cancer is a suitable medical application since the lymph nodes to be examined are located near the surface of the skin [4].

A single-sided MPI scanner capable of three-dimensional imaging with a field-free point (FFP) was built at the Institute of Medical Engineering in Luebeck (Figure 1). It was the first single-sided MPI scanner that has been built [3]. By adding two double-D shaped coil pairs, a second and third dimension in imaging has been added to the initially one-dimensional system [5–7].

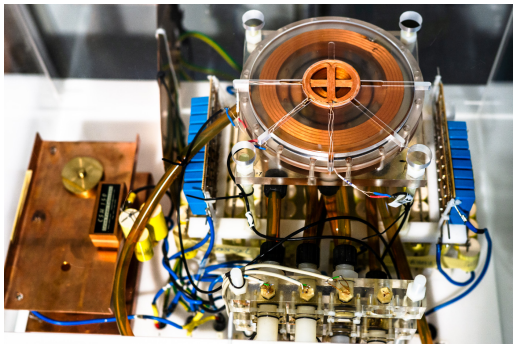

Figure 1: Top view of the Single Sided-Scanner at the Institute of Medical Engineering.

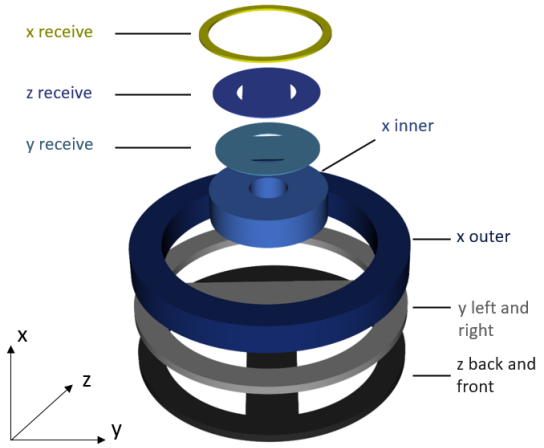

Figure 2: Explosion view of the three-dimensional single-sided FFP scanner with descriptions for each coil. The superposition of the fields generated by the coils *x inner* (transmit and selection field coil) and *x outer* (selection field coil) causes the generation of the FFP and the excitation in x-direction. The coils *y left and right* and *z back and front* are responsible for the FFP movement and the excitation in y- and z-direction.

Table 1: Scanner dimensions and used currents. The inner circular coil is simultaneously the transmit and selection field coil, the outer circular coil is used as selection field coil. The D-shaped coil pairs are used to move the FFP in y- and z-direction as well as for the excitation in those directions.

	inner circular coil	**outer circular coil**	**D-shaped coil pairs**
outer diameter	58 mm	140 mm	140 mm
inner diameter	19 mm	107.5 mm	114 mm
DC	65 A	55 A	-
AC_{peak}	42 A	-	80 A

There are different approaches of single-sided systems optimized for different medical applications. As an alternative to imaging with an FFP, the group of A. Tonyushkin developed a single-sided system that uses a field-free line (FFL) for imaging. Instead of using electromagnetic coils, this system uses permanent magnets to generate the selection field. With the help of additional electromagnetic coils and the rotation of the setup multi-dimensional imaging is possible [8–10]. An advantage of FFL systems over FFP systems is the overall higher sensitivity [11].

Recently, a single-sided system was presented by Mason et al. that is compact enough to be handheld and is capable of detecting magnetic particles but cannot be used for imaging. They propose a combination of this system with a small-bore MPI system to detect and rapidly examine breast cancer tumors [12]. One challenge faced by all single-sided MPI systems is the limited penetration depth that exists due to the inhomogeneous magnetic fields.

In this work phantom measurements, building on previous measurements to characterize the system [13, 14], are presented to determine the achievable penetration depth and spatial resolution in three-dimensional imaging. Additionally, the influence of the receiving coil orientation is investigated. To ensure that the measurement results obtained with the single-sided scanner are reproducible and can be quantified, a dilution study was performed, which is also presented in this work.

II. Methods and measurements

In this section the single-sided FFP MPI scanner is shortly introduced and the two- and three-dimensional measurements are proposed to further characterize the system behavior.

II.I. Single-Sided FFP Scanner

The single-sided scanner used for the presented measurements consists of three transmit coils, one for each channel respectively. With the three receiving coils, one for each channel, three-dimensional imaging is possible, see Figure 2. The size of each coil and the used currents are shown in Table 1. The respective DC signal is sent from the PC to the DC sources (SM 15-200D, Delta Electronika BV, Zierikzee, Netherlands) and passes through a feedthrough filter (GB.E2. 100A.AB.26.x.08, Bajong Electronic GmbH, Pilsting, Germany), to the inner and outer x-coil to generate the selection field. The three AC transmit chains describe the path of the signal from the IO boards (Innovative Integration, CA, USA) via an AC amplifier (DCU2250-28, MT MedTech Engineering GmbH, Berlin, Germany) and a bandpass filter to the respective transmit coils of the x-, y- and z-channel. The incoming signal is additionally sent back to the PC via a voltage

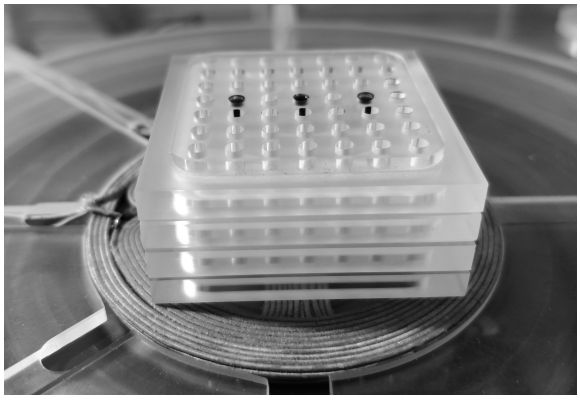

Figure 3: A photo of the four-layer-phantom that was used for measuring the penetration depth, the spatial resolution and for investigating the influence of the orientation of the receive coils.

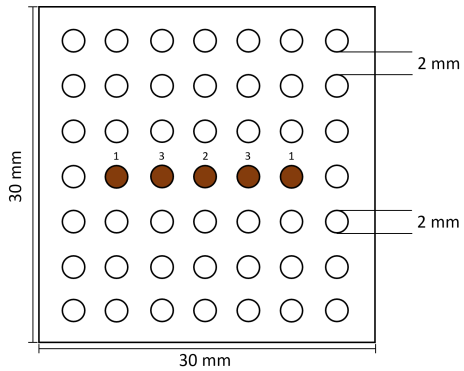

Figure 4: A sketch of the phantom that was used for measuring the penetration depth, the spatial resolution and for investigating the influence of the orientation of the receiving coils on the quality of the reconstructed images. To investigate the latter, the phantom was measured at different angles to the y-axis of the scanner. The numbers in the sketch represent the filling order.

divider for verification. The receive chain for each of the three channels consists of a notch filter, a low-noise amplifier, a single-to-differential converter and the 10-M IO card connected to the PC and clocked by a timing card [15].

II.II. Scanner configurations

A base frequency of $f_0 = 2.5$ MHz was used for excitation. For three-dimensional imaging, three frequency dividers, one for each channel, were chosen, $f_{dx} = 99$, $f_{dy} = 96$ and $f_{dz} = 93$. This led to the respective excitation frequencies $f_x \approx 25.25$ kHz, $f_y \approx 26.04$ kHz and $f_z \approx 26.88$ kHz. In the two-dimensional case the frequency dividers $f_{dx} = 99$ and $f_{dy} = 96$ led to the respective frequencies $f_x \approx 25.25$ kHz and $f_y \approx 26.04$ kHz.

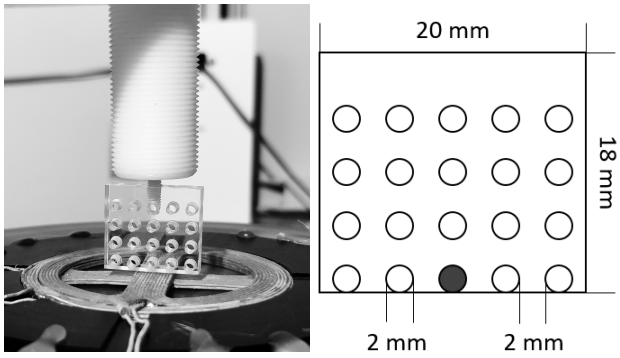

Figure 5: (left) A photo of the phantom that was used for the dilution study. (right) Sketch of the corresponding phantom with the marked position, that was filled with the diluted tracers.

II.III. Measurements

To determine the penetration depth and the spatial resolution of the single-sided scanner, a layer phantom (see Figure 3), which consists of four layers, was measured three-dimensionally. A second phantom was measured two-dimensionally in the dilution study to investigate the linear system response. Since the orientation of the receiving coils with respect to each other affects the magnetic fields generated, the signal quality could suffer from certain variations in the accuracy of the implementation of the coils. Therefore, measurements were performed to investigate the influence of the alignment of the receive coils by rotating and measuring the phantom at different angles.

II.III.1. Penetration depth and spatial resolution measurements

As published in [15], the penetration depth for three-dimensional imaging was 8 mm. Therefore a system matrix is measured in a FOV of 16 x 32 x 32 mm^3 and discretized in 8 x 16 x 16 positions.
The size of the four-layer phantom is 30 x 30 x 4 mm^3 with a total height of 17 mm when stuck together. The particles are located in the top layer 14 mm from the scanner surface. Each layer consists of 7 x 7 circular holes with a diameter of 2 mm and 2 mm height, each with a capacity of 7 µl.

First, two holes were filled with particles as shown in Figure 4. Four different angles, 0°, 22.5°, 45° and 90° to the x-axis of the scanner were measured to determine the influence of the orientation of the receive coils on the reconstructed image quality. The measurements were repeated with three filled holes and five filled holes respectively as demonstrated in Figure 4. The measurements were averaged 150 times.

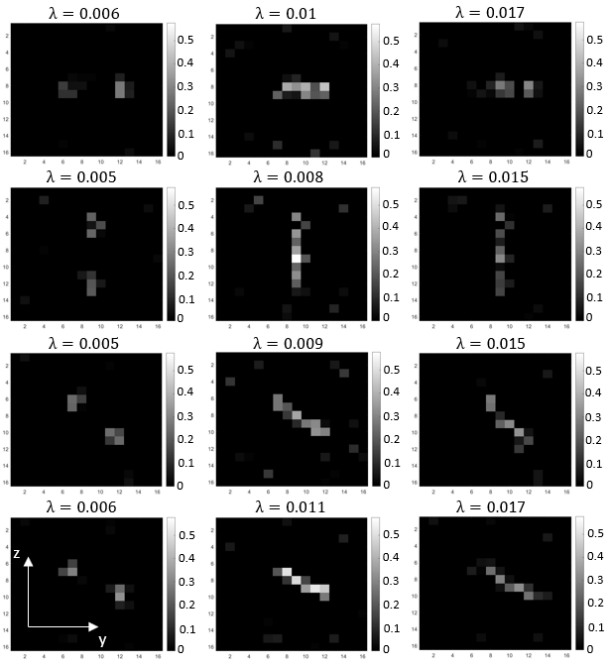

(a) Reconstructed images of layer one with a distance of 3.5 mm to the scanner surface. The results are normalized to the overall maximum signal.

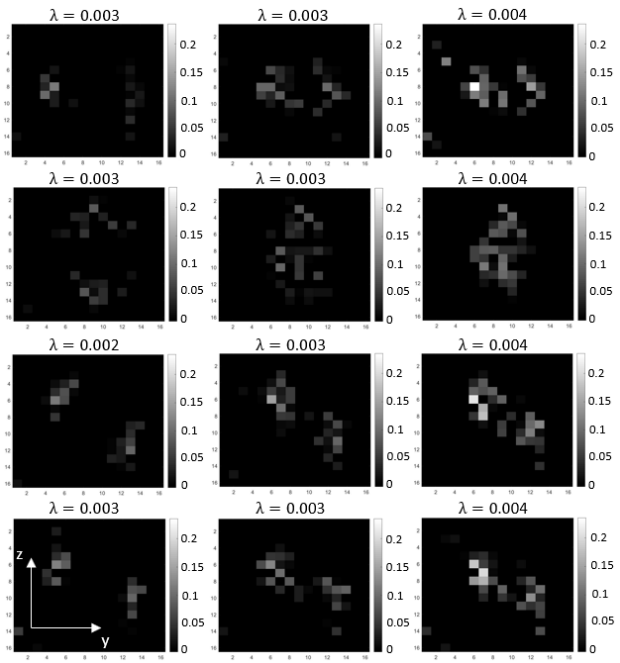

(b) Reconstructed images of the uppermost layer with a distance of 14 mm to the scanner surface. The results are normalized to the overall maximum signal.

Figure 6: Reconstructed results of the top and bottom phantom layer with the respective regularization parameter above the corresponding image. The left column shows two, the middle column three and the right column five filled positions in the phantom. The rows represent the four angles, 0°, 90°, 45° and 22.5° from top to bottom.

II.III.2. Linear system response measurements

To ensure that the measurement results that we get from the system are comparable, the linearity of the system response was investigated. Therefore, three different tracers, Resovist (Bayer Schering Pharma, Berlin, Germany; now distributed by FUJIFILM RI Pharma), Perimag (micromod, Rostock, Germany) and Synomag-S (micromod, Rostock, Germany) were chosen for a dilution study.

A system matrix was measured for each tracer on a FOV of 16 x 32 mm^3, which was discretized into 8 x 16 positions. For the measurements the particles were diluted in water from 0 % to 90 % dilution in 10 % increments. A phantom, that can be seen in Figure 5 was used for the two-dimensional measurements.

One hole in the phantom, that holds 10 µl, was filled and measured for each dilution step and each tracer with an averaging of 200 for each measurement. To varify the results, each measurement was repeated ten times.

II.IV. Reconstruction

To collect data from each position in the FOV, a system matrix S was measured for each of the selected tracers Perimag, Resovist and Synomag-S. For the system matrix acquisition a cube-shaped sample containing 8 µl of each tracer was used to measure the particle response at each position in the FOV. The linear equation

$$\hat{S}c = \hat{u} \tag{1}$$

describes an ill posed problem which can be solved with an iterative Kaczmarz algorithm. An SNR threshold was used to eliminate the frequency components that contained too much noise, resulting in a reduced system matrix $\hat{S}$ and measurement $\hat{u}$. c represents the desired particle concentration. To calculate the SNR, the row energy of each frequency component at the spatial position r was determined,

$$w_{f,r} = \|(SP_{f,r} - SE_{f,r})\|, \tag{2}$$

where SP is the system matrix measured with particles, and SE is the system matrix measured without particles. With the standard deviation σ of SE this results in

$$SNR = \frac{w_{f,r}}{\sigma_f}. \tag{3}$$

A weighting diagonal matrix

$$W = diag(\frac{1}{w_{f_r}^2}), \tag{4}$$

which consists of the reciprocal of the squared row energy of S, and a Tikhonov-regularization to stabilize the

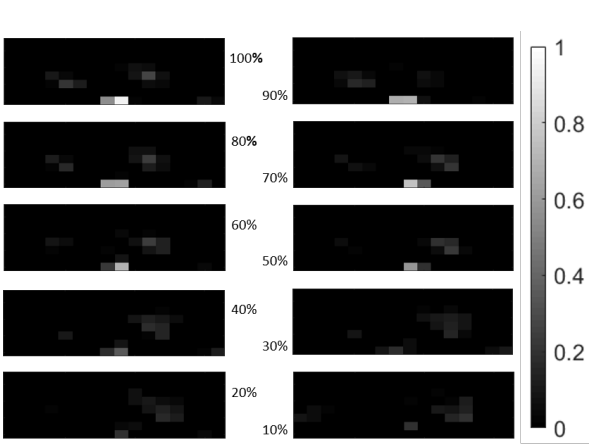

(a) Resovist reconstructed results.

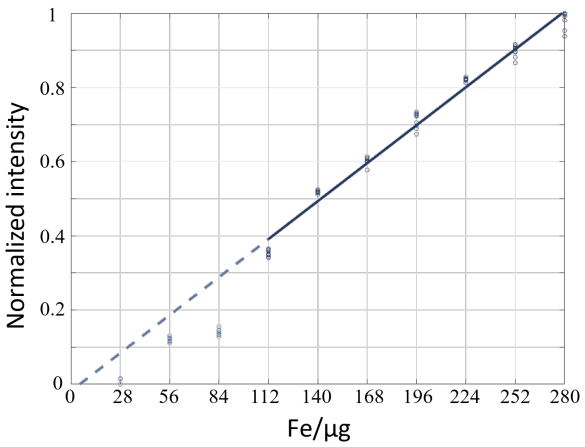

(b) Resovist plot of the intensities at each dilution step. Down to 112 µg iron the system responds linearly.

Figure 7: The left image shows the reconstructed results of every dilution step for Resovist. 100 % represents the reconstruction of the undiluted tracer. The plot on the right shows the signal of the corresponding phantom positions at each dilution step normalized to the maximum signal of the reconstructed undiluted tracer measurement respectively.

results are used to address the ill posed problem. The final equation to be solved is as follows

$$(\hat{S}^* W \hat{S} + \lambda I)c = \hat{S}^* W \hat{u}, \tag{5}$$

where $\hat{S}^*$ represents the conjugate transpose of the reduced system matrix and I the identitiy matrix [5].

III. Results

The reconstructions of the measurements presented above are shown and described in this chapter.

III.I. Penetration depth and spatial resolution measurement results

For reconstruction, the regularization factor λ was calculated for each measurement individually [5]. Each of the four layers, in which the first two, then three and finally five holes were filled with particles, was measured three-dimensionally at four angles, resulting in a total of 48 measurements. The maximum distance between the particles and the scanner surface was 14 mm, the minimum distance was 3.5 mm. Figure 6a shows the reconstructed images from the measurement of the layer closest to the scanner surface. From the first to the last row, the phantom is shown at an angle from 0° to 90°. From the left to the right column, the number of filled holes increases from two to five. Figure 6b shows the top layer for the corresponding angles and filled holes in the phantom.

III.II. Orientation of the receiving coils measurement results

For the investigation of the influence of the orientation of the receiving coils, the reconstructions of the uppermost and the bottom layer of the phantom are shown in Figure 6.

III.III. Linear system response measurement results

The reconstruction algorithm with 500 iteration steps was used and a constant regularization parameter λ was chosen for optimal comparison of the results. The reconstructed images of selected dilution steps for Resovist are shown in Figure 7a, for Perimag in Figure 8a and for Synomag-S in Figure 9a. Each of the three tracers was diluted in 10 steps and measured successively. The measurement was repeated 10 times for each dilution, resulting in a total of 300 measurements. The reconstructed images show the averaged signal intensities of the tracer positions. The plots of the measured signal intensities for each of the tracers are shown in Figures 7b, 8b and 9b.

IV. Discussion

The results of the measurements described above are discussed in this chapter.

10.18416/ijmpi.2021.2109001

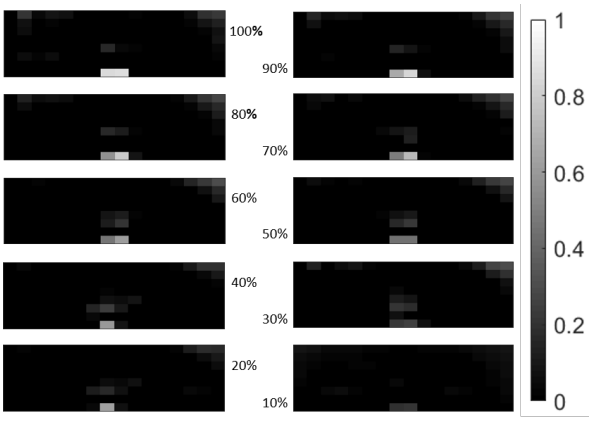

(a) Perimag reconstructed results.

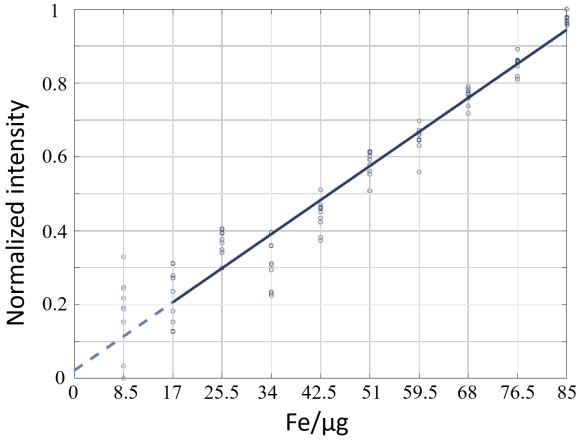

(b) Perimag plot of the intensities at each dilution step. The regression line shows a linear course of the tracer down to 17 µg iron in the dilution.

Figure 8: The left image shows the reconstructed results of every dilution step for Perimag. 100 % represents the reconstruction of the undiluted tracer. The plot on the right shows the signal of the corresponding phantom positions at each dilution step normalized to the maximum signal of the reconstructed undiluted tracer measurement respectively.

IV.I. Penetration depth and spatial resolution

For the reconstruction 200 iteration steps were chosen, because this provided the best image quality after visual inspection. The appropriate selection of iteration steps and other parameters for the reconstruction has a decisive influence on the image quality. It can be clearly seen that the resolution in y- and z-direction decreases with the distance to the scanner surface. The two filled holes of the top layer can be distinguished, but the images contain a lot of noise. To judge whether the signal differs significantly from the noise, an empty measurement was reconstructed and the highest noise signal was lower by a factor of 10 than the measured particle signal at a distance of 14 mm. For this reason we can speak of a penetration depth of 14 mm to the scanner surface. In three-dimensional imaging, the spatial resolution in y- and z-direction is lower than in x-direction, since in y- and z-direction a weaker gradient field is generated due to the coil arrangements [16]. Possibly coupling effects contribute to the fact that the spatial resolution is lower in three-dimensional imaging than in two-dimensional imaging.

IV.II. Orientation of the receiving coils

There are no visible differences in the quality of the reconstructed images from different angles. This means that the measured angle of the phantom to the y-axis of the scanner and therefore the orientation of the receiving coils has no visible influence on the quality of the reconstructed images. This shows that the receiving coils have been accurately installed and are precisely located so that they receive the generated signal synchronously. We designed the measurements explicitly for this study, which represent an important part of characterizing the system behavior.

IV.III. Linear system response

For quantification of measurement results, the linear system behavior must be ensured [17]. Therefore a dilution study was performed to show, that the measurement results are reproducable. In addition to Resovist, two other tracers were selected to strengthen the results, since it appears that Resovist does not behave linearly at linear dilution [18]. Contrary to this assumption, our results show a linear system response for all three selected tracers down to a dilution of 112 µg iron for Resovist, 17 µg iron for Perimag and down to 40 µg iron in the dilution for Synomag-S, whereas Synomag-S showed the best results in the reconstructed signal intensities. The quantifiability of the results for the examined system is thus given.

V. Conclusion and Outlook

A conclusion is drawn for each of the presented measurements based on the presented results. A respective outlook is described for the individual case.

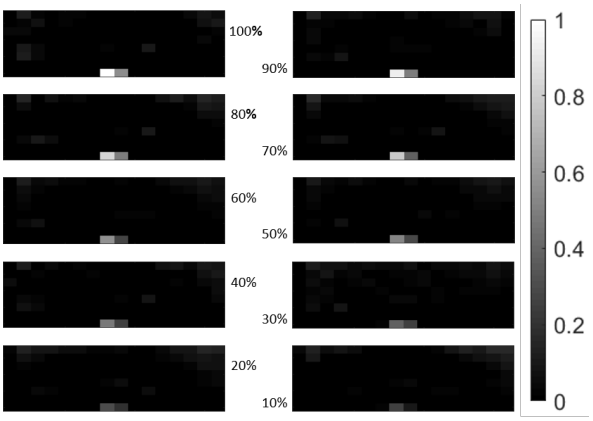

(a) Synomag-S reconstructed results.

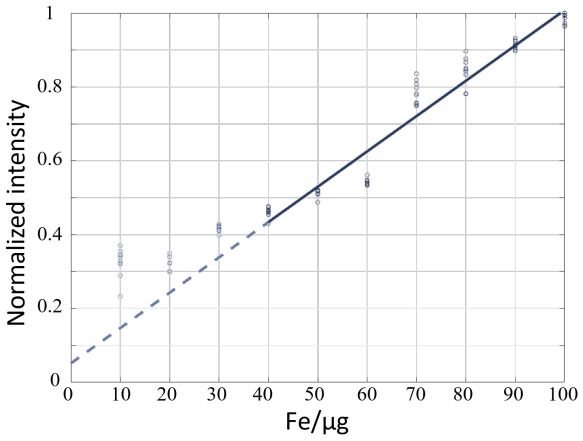

(b) Synomag-S plot of the intensities at each dilution step. The regression line was calculated from the measurements down to 40 µg iron in the dilution and shows a linear course.

Figure 9: The left image shows the reconstructed results of every dilution step for Synomag-S. 100 % represents the reconstruction of the undiluted tracer. The plot on the right shows the signal of the corresponding phantom positions at each dilution step normalized to the maximum signal of the reconstructed undiluted tracer measurement respectively.

V.I. Penetration depth and spatial resolution

Up to 14 mm distance to the scanner surface, the two tracer-filled positions in the phantom could be distinguished. The images are noisy compared to the reconstructions of the first layer, which is caused by the decreasing magnetic field due to the one sided arrangement of the system. Our results show that it is possible to distinguish particles in a distance of 14 mm to each other in this distance to the scanner surface. Since we have measured that the noise level is significantly lower than the measurable particle signal at that distance, the penetration depth of the system is 14 mm. The spatial resolution in z- and y-direction is at least 14 mm, but since the step from 14 mm to 6 mm can be further decreased, further measurements have to be done to investigate if the spatial resolution lies between 6 mm and 14 mm.

V.II. Orientation of the receiving coils

A visual examination of the reconstructed images showed no influence of the measured angle of the phantom to the y-axis of the scanner and therefore the orientation of the receive coils in y- and z-direction. This is an important finding because we can assume that the influence of the different coils in the system is uniform, and thus we can assume that our system will not cause fluctuations in the reconstructed signal when making measurements across the FOV.

V.III. Linear system response

The dilution study was a necessary step to quantify the measurement results and to further characterize the system properties. The more system properties are known, the better the reconstructed results can be understood. Thus, one gets the possibility to influence the results with the help of the gained knowledge about the scanner behavior. In addition, we obtain precise knowledge about which objects we can measure without problems and for which we can expect good results. Furthermore, we can plan possible improvements to the system from the knowledge gained. Further measurements will follow, which underline the results presented here and strengthen the validity of the results.

Acknowledgments

The authors thank the German Federal Ministry of Education and Research (01DL17010A) for financial support.

References

[1] B. Gleich and J. Weizenecker. Tomographic imaging using the nonlinear response of magnetic particles. *Nature*, 435(7046):1214–1217, 2005, doi:10.1038/nature03808.

[2] T. Knopp, S. Biederer, T. F. Sattel, J. Weizenecker, B. Gleich, J. Borgert, and T. M. Buzug. Trajectory analysis for magnetic particle imaging. *Physics in Medicine and Biology*, 54(2):385–397, 2009, doi:10.1088/0031-9155/54/2/014.

[3] T. F. Sattel, T. Knopp, S. Biederer, B. Gleich, J. Weizenecker, J. Borgert, and T. M. Buzug. Single-sided device for magnetic particle imaging. *Journal of Physics D: Applied Physics*, 42(2):022001, 2008, doi:10.1088/0022-3727/42/2/022001.

[4] D. Finas, K. Baumann, L. Sydow, K. Heinrich, A. Rody, K. Grafe, T. M. Buzug, and K. Ludtke-Buzug. SPIO Detection and Distribution in Biological Tissue - A Murine MPI-SLNB Breast Cancer Model. *IEEE Transactions on Magnetics*, 51(2):1–4, 2015, doi:10.1109/TMAG.2014.2358272.

[5] K. Gräfe, A. von Gladiss, G. Bringout, M. Ahlborg, and T. M. Buzug. 2D Images Recorded With a Single-Sided Magnetic Particle Imaging Scanner. *IEEE Transactions on Medical Imaging*, 35(4):1056–1065, 2016, doi:10.1109/TMI.2015.2507187.

[6] K. Gräfe, A. von Gladiss, and T. M. Buzug, First Phantom Measurements with a 3D Single Sided MPI Scanner, in *International Workshop on Magnetic Particle Imaging*, 2018.

[7] A. von Gladiss, Y. Blancke Soares, T. M. Buzug, and K. Gräfe, Dynamic Imaging with a 3D Single-Sided MPI Scanner, in *International Workshop on Magnetic Particle Imaging*, 235–236, 2019.

[8] G. Rudd and A. Tonyushkin. Design of a Permanent Magnet Selection Field Structure for a Single-Sided Field-Free Line Magnetic Particle Imaging Scanner. *International Journal on Magnetic Particle Imaging*, 4(1), 2018, doi:10.18416/IJMPI.2018.1809001.

[9] A. Tonyushkin. Single-Sided Field-Free Line Generator Magnet for Multi-Dimensional Magnetic Particle Imaging. *IEEE Transactions on Magnetics*, 53(9):1–6, 2017, doi:10.1109/TMAG.2017.2718485.

[10] J. Pagan, C. McDonough, T. Vo, and A. Tonyushkin. Single-Sided Magnetic Particle Imaging Device With Field-Free-Line Geometry for In Vivo Imaging Applications. *IEEE Transactions on Magnetics*, 57(2):1–5, 2021, doi:10.1109/TMAG.2020.3008596.

[11] J. Weizenecker, B. Gleich, and J. Borgert. Magnetic particle imaging using a field free line. *Journal of Physics D: Applied Physics*, 41(10):105009, 2008, doi:10.1088/0022-3727/41/10/105009.

[12] E. E. Mason, E. Mattingly, K. Herb, M. Śliwiak, S. Franconi, C. Z. Cooley, P. J. Slanetz, and L. L. Wald. Concept for using magnetic particle imaging for intraoperative margin analysis in breast-conserving surgery. *Scientific Reports*, 11(1):13456, 2021, doi:10.1038/s41598-021-92644-8.

[13] Y. Blancke Soares, K. Gräfe, A. von Gladiss, C. Debbeler, K. Lüdtke-Buzug, and T. M. Buzug, Verification of the Linear System Response of a Single-Sided MPI Device, in *International Workshop on Magnetic Particle Imaging*, 51–52, 2019.

[14] Y. Blancke Soares, K. Gräfe, K. Lüdtke-Buzug, and T. M. Buzug, Investigation of the spatial resolution and penetration depth of a single-sided MPI device in three-dimensional imaging, in *International Workshop on Magnetic Particle Imaging*, 2020. doi:10.18416/IJMPI.2020.2009053.

[15] K. Gräfe, Bildgebungskonzepte für Magnetic Particle Imaging Magnetic Particle Imaging mit einer asymmetrischen Spulentopologie. Lübeck: Infinite Science Publishing, 2016, ISBN: 978-3-945954-27-0.

[16] K. Gräfe, M. Grüttner, T. F. Sattel, M. Graeser, and T. M. Buzug, Single-sided magnetic particle imaging: magnetic field and gradient, in *SPIE Medical Imaging*, J. B. Weaver and R. C. Molthen, Eds., 867219, 2013. doi:10.1117/12.2001610.

[17] O. Kosch, U. Heinen, L. Trahms, and F. Wiekhorst. Preparing system functions for quantitative MPI. *International Journal on Magnetic Particle Imaging*, 3(2), 2017, doi:10.18416/IJMPI.2017.1706002.

[18] N. Löwa, P. Radon, O. Kosch, and F. Wiekhorst. Concentration Dependent MPI Tracer Performance. *International Journal on Magnetic Particle Imaging*, 2(1), 2016, doi:10.18416/IJMPI.2016.1601001.

